Author's personal copy

Journal of Crystal Growth 338 (2012) 96–102

Contents lists available at SciVerse ScienceDirect

Journal of Crystal Growth

journal homepage: www.elsevier.com/locate/jcrysgro

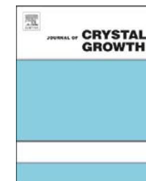

Synthesis of vanadium dioxide thin films on conducting oxides and metal–insulator transition characteristics

Yanjie Cui [a,*], Xinwei Wang [b], You Zhou [a], Roy Gordon [b], Shriram Ramanathan [a]

[a] Harvard School of Engineering and Applied Sciences, Harvard University, Cambridge, MA 02138, USA
[b] Harvard Department of Chemistry and Chemical Biology, Harvard University, Cambridge, MA 02138, USA

ARTICLE INFO

Article history:
Received 18 September 2011
Received in revised form
6 October 2011
Accepted 20 October 2011
Communicated by S. Uda
Available online 29 October 2011

Keywords:
A1. Characterization
A1. Substrates
A3. Physical vapor deposition processes
B1. VO_2
B2. Metal–insulator transition materials

ABSTRACT

We report on growth and physical properties of vanadium dioxide (VO_2) films on model conducting oxide underlayers (Nb-doped $SrTiO_3$ and RuO_2 buffered TiO_2 single crystals). The VO_2 films, synthesized by rf sputtering, are highly textured as seen from X-ray diffraction. The VO_2 film grown on Nb doped $SrTiO_3$ shows over two orders of magnitude metal–insulator transition, while VO_2 film on RuO_2 buffered TiO_2 shows a smaller resistance change but with an interesting two step transition. X-ray photoelectron spectroscopy has been performed as a function of depth on both sets of structures to provide mechanistic understanding of the transition characteristics. We then investigate voltage-driven transition in the VO_2 films grown on Nb-doped $SrTiO_3$ substrate as a function of temperature. The present study contributes to efforts towards correlated oxide electronics utilizing phase transitions.
© 2011 Elsevier B.V. All rights reserved.

1. Introduction

Vanadium dioxide shows a metal–insulator transition (MIT) with several orders of magnitude conductivity change, accompanied by a phase change from high temperature tetragonal rutile structure ($P4_2/mnm$) to low temperature monoclinic structure ($P2_1/c$) [1]. The phase change is accomplished by a small lattice distortion along the *c* axis of the tetragonal structure hence the formation of V–V pairs along *a* axis in the monoclinic structure. The transition temperature could be manipulated to either higher or lower temperature through cation substitution as investigated early in late 60's, for example: W^{6+}, Nb^{5+}, Ru^{4+} etc. most higher valence state ($\geq 4+$ except Ge^{4+}) cation doping depress the transition temperature, while M^{3+} (M=Cr, Fe, Ga, Al) doping elevates the transition temperature [2].

It is necessary to be able to deposit high quality VO_2 films on conducting substrates in order to explore carrier conduction out-of-plane of the film. To date, VO_2 films have primarily been grown on conducting substrates such as heavily-doped Si or Ge, and Pt [3–5]. As far as conducting oxide substrates are concerned, there is a recent report discussing the role of twin boundaries of VO_2 grown on Ga-doped ZnO buffered *c*-sapphire [6]. VO_2 films grown on conducting oxides would be of particular interest to explore all-oxide electronics wherein the underlayer could be used as an electrode for electron transport. Therefore, here we have studied the physical properties of VO_2 grown on conducting oxide substrates namely Nb-doped $SrTiO_3$ single crystal substrate and RuO_2 buffered TiO_2 single crystal substrate.

2. Experimental

VO_2 thin films ($\sim$200 nm) were deposited by rf-sputtering on two representative conducting oxide substrates: Nb-doped $SrTiO_3$ (001) (Nb:STO) or RuO_2 (101) buffered TiO_2 (101) single crystal substrates. The single crystals of Nb:STO (Nb weight concentration 1.0%) with resistivity of 0.0035 Ω cm were used as-obtained (from MTI Crystal) except for high pressure nitrogen cleaning before loading into a sputtering chamber. Crystalline RuO_2 thin films were grown by pulsed chemical vapor deposition in a home-built tube reactor [7], with bis(N,N′-di-tert-butylacetamidinato) ruthenium (II) dicarbonyl as the ruthenium precursor and oxygen as co-reactant gas. The ruthenium precursor was placed in a glass bubbler in an oven set at 140 °C, and it was delivered into the reactor tube with nitrogen as carrier gas in each precursor pulse. The precursor has a vapor pressure of 100 mTorr at 140 °C, and the glass bubbler has a volume of 0.14 L, therefore, an amount of 14 mTorr L precursor vapor was delivered during each pulse. While the ruthenium precursor was delivered, a gas mixture of oxygen and nitrogen (O_2:N_2=1:2 in partial pressure) was kept flowing at a total pressure of 450 mTorr. The deposition temperature was 280 °C. Given the pumping speed of 2.5 L/s, the exposure of the ruthenium precursor was estimated to be approximately

* Corresponding author. Tel.: +1 617 797 4285.
E-mail address: cuiyanjie@hotmail.com (Y. Cui).

0022-0248/$ - see front matter © 2011 Elsevier B.V. All rights reserved.
doi:10.1016/j.jcrysgro.2011.10.025

Author's personal copy

7.5 mTorr s for each pulse. Several hundred pulses of ruthenium precursor were supplied to grow the RuO_2 film. Rutile TiO_2 (101) substrates supplied by MTI Corporation were used for growing epitaxial RuO_2 films. Each substrate was treated with UV/ozone for 5 min to remove surface organic contaminants before deposition. The RuO_2 film thickness is ~38 nm with resistivity of 0.00008 Ω cm. The sputtering was performed in an Ar environment at a set pressure of 10 mTorr from a V_2O_5 target for 6 h, with the substrate temperature and RF source power set at 550 °C and 120 W, respectively. Detailed description of VO_2 film growth by sputtering and deposition condition effects on properties can be found in the previous reports [4,8].

X-ray diffraction (XRD) experiments were first characterized by the Bruker D8, which has a conventional 1.6 kW sealed X-ray tube source, a horizontal circle Eulerian cradle and a Vantec2000 2D detector. The data were collected with 0.3 mm monocapillary lenses and a graphite monochromator at the incident-beam side. The VO_2 film on RuO_2 was further characterized by a triple-axis diffractometer, the Bruker D8 high resolution XRD (HRXRD) diffractometer, with Cu $K\alpha$ radiation, configured with a Göbel mirror and a Ge(022) × 4 asymmetric monochromator at the incident-beam side, and the Pathfinder, a scintillation point detector, at the receiving-side. Crystallographic characterization was accomplished with 2θ–ω coupled scans, and a ϕ scan (for epitaxial film only). A Zeiss Ultra 55 Field Emission Scanning Electron Microscope (FESEM) was employed to obtain microstructures and operated at 5 keV with in-lens detector. X-ray photoelectron spectroscopy (XPS) measurements were performed in an ESCA SSX-100 spectrometer with Al $K\alpha$ (1.4866 keV) as the X-ray source. XPS depth profiling was assisted with Ar ion milling with spectra taken after every 10 min etching. All the XPS data were analyzed with Casa-XPS software package. Au (200 nm)/Ti (20 nm) metal contacts with different sizes ranging from 50 × 50 μm^2 to 500 × 500 μm^2 were deposited in a Denton E-Beam Evaporator with shadow mask. The electrical properties were measured in a probe station equipped with a hot stage and a Keithley 236 source meter.

3. Results and discussion

Fig. 1 shows the 2θ–ω coupled X-ray diffraction patterns for VO_2 film grown on Nb:STO single crystals substrate and RuO_2 buffered TiO_2 single crystal substrates. The VO_2 film on Nb:STO is highly textured, as seen in Fig. 1a, the major peaks at 27.83°, 57.44° 2θ are attributed to the reflection of (011) and (022) plane of the monoclinic phase, and the other minor peaks belong to VO_2 or the substrate. The high-resolution XRD characterization of VO_2 film on RuO_2 is shown in Fig. 1b. The peaks at 35.77°, 36.11°, 37.13°, are ascribed to (101) plane of tetragonal RuO_2, TiO_2 and VO_2, respectively. The as-deposited RuO_2 (101) diffraction in the epitaxial film shifts from 35.05° (for bulk single crystal) to 35.54° approaching the substrate TiO_2 (101) diffraction (at 36.08° for single crystal). This indicates that the RuO_2 d_{101} spacing is decreasing dominated by the decrease of the c axis of RuO_2 to match the substrate lattice (crystallographic information is shown in Table 1 [9–12]). After the VO_2 growth, the RuO_2 (101) peak further shifted towards higher angles at 35.77°. The in-plane orientation was determined from ϕ scan on (002) plane for both TiO_2 substrate and VO_2 film, suggesting epitaxial growth of VO_2 on the RuO_2 buffered TiO_2 substrate, as shown in Fig. 2b inset.

Field emission SEM images show the morphology of the films grown on different substrates (Fig. 2a,b). In Fig. 2a, the "flower" like microstructure of VO_2 film on Nb:STO are composed of closely packed thin sheets, which could cause the highly oriented XRD patterns showed earlier. VO_2 film on RuO_2 buffered TiO_2 shows inclined column structure with a larger grain size of about

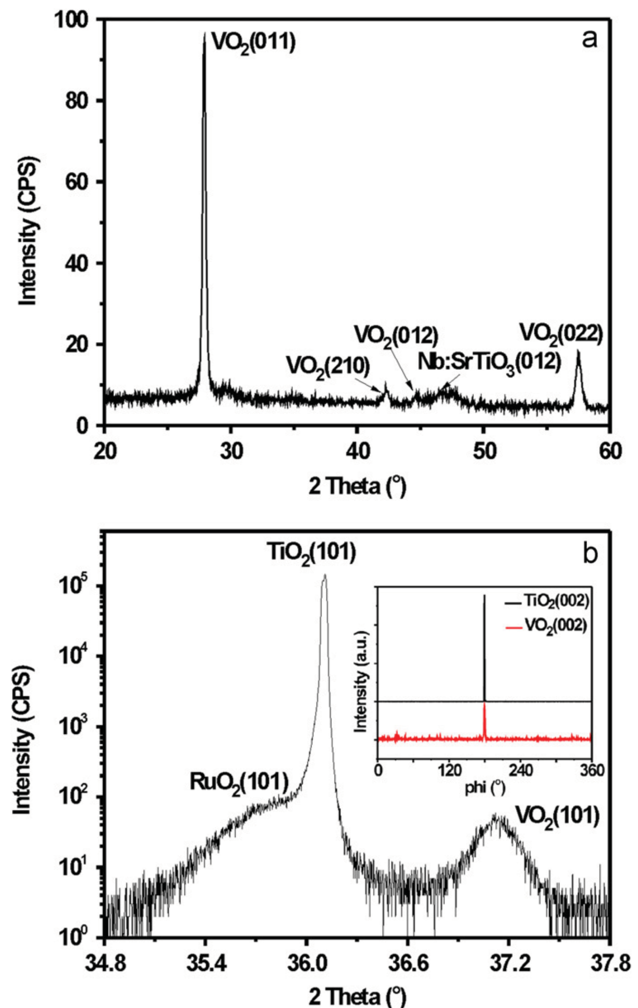

Fig. 1. 2θ–ω scan X-ray diffraction patterns of VO_2 films grown on different substrates: (a) VO_2 on Nb-doped $SrTiO_3$ (001) (VNST) and (b) VO_2 on RuO_2 buffered TiO_2 (101) (VRT). Inset in (b) is the ϕ scan of (002) plane of film VO_2 and substrate TiO_2.

Table 1
Lattice parameters of various materials considered in this study.

Substrates	Space group	Lattice parameter (Å)	
		a	c
$SrTiO_3$	Pm-3m	3.905	-
TiO_2	$P4_2/mnm$	4.594	2.959
RuO_2	$P4_2/mnm$	4.492	3.106
VO_2 (HT)	$P4_2/mnm$	4.554	2.856
VO_2 (LT)	$P2_1/c$	a: 5.753, b: 4.526	5.383

200 nm. Both films exhibit well defined crystalline grains, and the uniformity was checked by taking images across several regions. The thickness of both VO_2 film on Nb:STO or RuO_2 buffered TiO_2 are ~200 nm as shown in SEM micrographs from film cross-section, Fig. 2c,d. From Fig. 2d, we can observe that the RuO_2 buffer layer is ~35 nm.

The electrical properties of VO_2 films grown on Nb:STO and RuO_2 layer were characterized in both in-plane and out-of-plane geometry, as shown in Fig. 3, the normalized resistance ($R_n = R(T)/R$ (25 °C)) versus temperature curves (inset shows linear I–V curves

Author's personal copy

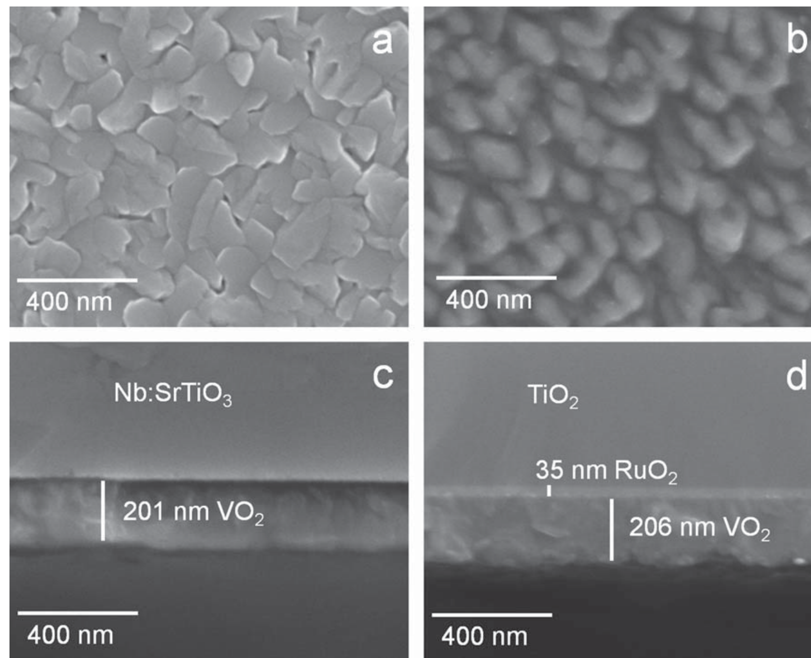

Fig. 2. Plan view and cross-section FESEM images of as-deposited VO_2 films grown on different substrates: (a, c) Nb-doped $SrTiO_3$, (b, d) RuO_2 buffered TiO_2.

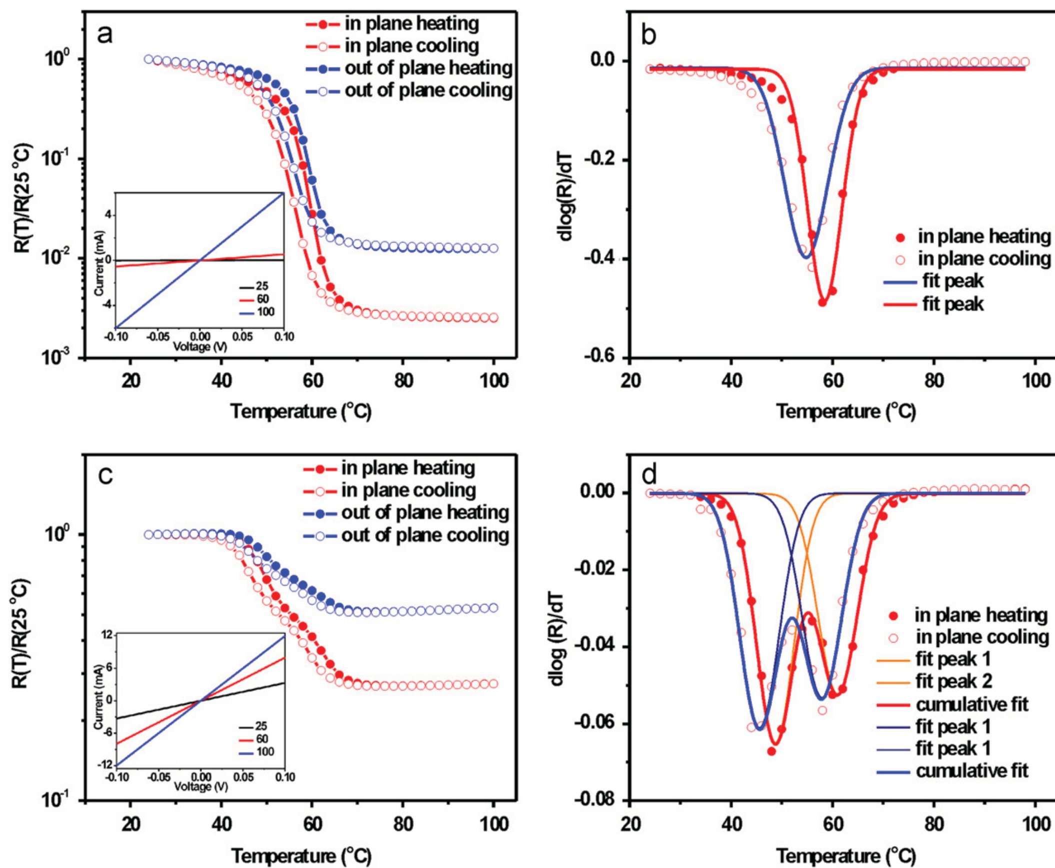

Fig. 3. (a) Normalized resistance plotted as a function of temperature for VO_2 films grown on Nb doped $SrTiO_3$, (b) derivative plot for in-plane measurement from which we extract the phase transition characteristics (c) normalized resistance plot for VO_2 grown on RuO_2 buffered TiO_2, insets show the derivative curves for the in-plane measurement and (d) corresponding derivative plot of in-plane resistance versus temperature Table 2 summarizes the phase transition characteristics.

Author's personal copy

from which the resistance values were determined). For VO_2 films on Nb:STO, the MIT temperature (T_{MIT}), defined as the peak position in the derivative curve of corresponding resistance versus temperature curve, was determined to be ~58.5 °C and 54.8 °C for heating and cooling from the in-plane measurement, as shown in Fig. 3b. The out-of-plane measurement shows similar T_{MIT} with ~58.1 °C and 54.4 °C for heating and cooling process, respectively, detailed MIT characteristics are summarized in Table 2. In Fig. 3a, in plane $R_n \sim T$ measurement of the VO_2 film on Nb:STO shows a larger resistance ratio ($\Delta A = R$ (25 °C)/R(100 °C)) of 397 compared to the out of plane ratio of 79. The lower transition order for out-of-plane measurement was also observed in a recent study, which discussed the twin boundary effect on MIT thermal hysteresis [6]. Yang et al. described that the thermal hysteresis of the out of plane measurement of epitaxial growth VO_2 on Ga:ZnO buffered *c*-sapphire with current flow parallel to the twin boundaries was considerably reduced compared to in plane measurement of epitaxial growth VO_2 on ZnO buffered *c*-sapphire where current flows normal to the boundaries. However, the thermal hysteresis (ΔH: difference between the critical temperature of heating and cooling curves) of the VO_2 film on Nb:STO for both in plane and out of plane measurement is similar, i.e. ~3.7 °C, which could be explained by the textured nature of our film.

Fig. 3c shows the $R_n \sim T$ curves of VO_2 film on RuO_2 buffered TiO_2 measured in both in-plane and out-of-plane geometry (inset shows representative linear *I–V* plots). This film shows a small resistance change in both in-plane and out-of-plane measurement compared to VO_2 films grown on Nb:STO deposited at the same time. The current flow in the low resistivity RuO_2 layer could explain the small resistance change for the in-plane measurement of a high quality VO_2 film, while this does not necessarily explain the small resistance change observed in the out of plane measurement. Since the phase transition is quite sensitive to stoichiometry, this smaller transition might indicate that this film is off-stoichiometric. It is interesting to note that this film shows a two step transition, as shown in Fig. 3d (derivative curve of the in-plane measurement, with two transitions at 48.7 and 61.0 °C during heating, and 45.6 and 57.9 °C during cooling, respectively).

Table 2
Phase transition characteristics of VO_2 films grown on different substrates.

Substrates	T_{MIT} (°C)	ΔH (°C)	ΔA	ΔT (°C)
Nb:$SrTiO_3$ (001)	58.5 (H), 54.8 (C)	3.7 in plane	397	8.0/10.1
Nb:$SrTiO_3$ (001)	58.1 (H), 54.4 (C)	3.7 out plane	79	7.4/9.3
RuO_2 (101)	48.7 (H), 45.6 (C) 61.0 (H), 57.9 (C)	3.1 in plane	3.6	8.7/9.1 9.1/9.2
RuO_2 (101)	48.5 (H), 46.0(C) 59.8 (H), 57.3 (C)	2.5 out plane	1.9	8.6/9.2 12.0/10.3

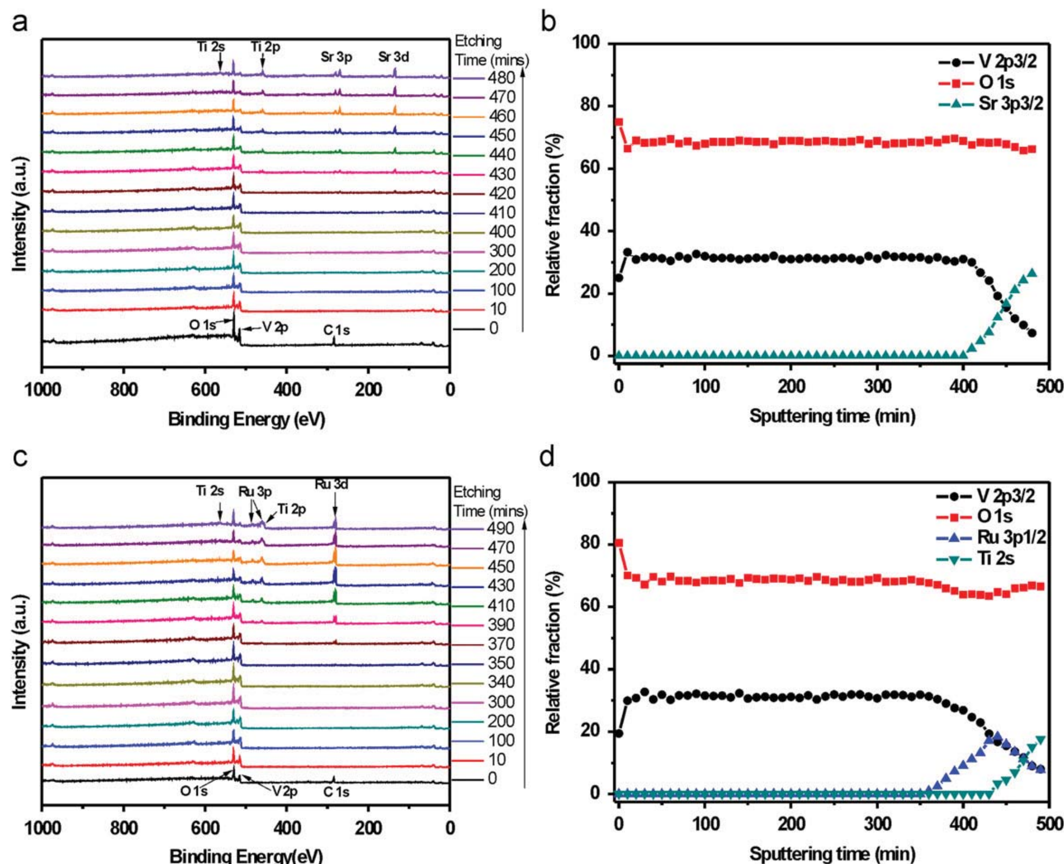

Fig. 4. XPS spectra of VO_2 films grown on: (a) Nb-doped $SrTiO_3$, (c) RuO_2 buffered TiO_2 and compositional depth profile of VO_2 film on: (b) Nb-doped $SrTiO_3$, (d) RuO_2 buffered TiO_2.

Author's personal copy

The transition width (ΔT: full width at half maximum of derivative curve) for these four peaks ranges from 8.7 to 9.2 °C, and the width of thermal hysteresis for both transition is 3.1 °C. The out-of-plane measurement shows the same two step transition with the T_{MIT} at 48.5 and 59.8 °C during heating, and 46.0 and 57.3 °C during cooling, respectively. The thermal hysteresis widths for both transitions in the out-of-plane measurement are 2.5 °C, which is narrower than the in plane measurement. This is consistent with the recent study that out of plane measurement shows narrower width of thermal hysteresis due to less grain boundaries in a columnar growth epitaxial film containing twin boundaries [6].

X-ray photoelectron spectroscopy (XPS) depth profiling was carried out on both sets of VO_2 films grown on Nb:STO and RuO_2 buffered TiO_2, as shown in Fig. 4. In the surface full scan spectra, except for the features arising from V and O, there are also N 1*s* and C 1*s*, which arises from surface contamination and Au from electrode fabrication. The adventitious C 1*s* peak was assumed to have a binding energy of 284.8 eV [13], and used to calibrate the binding energy of vanadium. High resolution XPS spectra were focused around the O 1*s* and V 2*p* region.

Fig. 4a and c shows the depth dependent XPS full scan spectra of VO_2 film on different substrates with the depth indicated by etching time, the curves are vertically shifted for clarity. The etching rate for VO_2 was calibrated to be ~0.5 nm/min. The distance (d) to the surface is estimated according to the etch rate and time. Fig. 4b summarizes the elements V, O and Sr concentration profile, which is calculated according to the relative sensitivity factor (RSF)-scaled areas under V $2p_{3/2}$, O 2*s* and Sr $3p_{3/2}$ peaks after the Shirley background subtraction. Due to any preferential sputtering rate of different elements, the absolute values of the atomic percentage may not be accurate, and hence we just compare the relative peak to peak intensity here. Both oxygen and vanadium are evenly distributed in the bulk part of the film (15–200 nm from surface). The fraction of V decreased from about 30% after 410 min etching to 15% after 450 min etching and the relative fraction of Sr correspondingly increase to 17% after 450 min etching. The slow decreasing rate (the profile tail) is commonly observed in the XPS depth profiling [14,15], since surface roughness as well as etching spot edge effect may blur the profile.

For VO_2 film on RuO_2 buffered TiO_2, as shown in Fig. 4c, the Ru peaks appeared after 350 min etching at ~175 nm to the surface. Then the intensity of Ru peak continuously increased to 18% until 440 min etching with the presence of Ti peak in the spectra. Fig. 4d summarized the relative fraction of the elements calculated according to the RSF-scaled areas under V $2p_{3/2}$, O 2*s*, Ru $3p_{1/2}$ and Ti 2*s* peaks. The V fraction decreased from 31% to 17% in 90 min etching from the observation of Ru peaks (after 350 min etching) to the presence of Ti peaks (after 440 min etching) from TiO_2 substrate. The etching rate of RuO_2 film on TiO_2 was calibrated to be ~1 nm/min based on both as deposited film and the film annealed under the VO_2 film deposition condition. From SEM image in Fig. 2d, we measured the thickness of RuO_2 layer is approximately 35 nm, which should be etched through in ~40 min. We, however, see that it takes 90 min from the observation of Ru to the observation of Ti peak. This difference and the slower decreasing rate of V concentration compared to the film on Nb:STO suggest that a solid solution, $V_{1-x}Ru_xO_2$, is likely formed at the interface. In addition, the VO_2 film is ~206 nm thick as shown in the SEM cross-section image, while we start to observe Ru peak at ~175 nm. Ru might diffuse into the VO_2 layer to the extent of ~30 nm (which is expected to take about 50 min etch time), and is consistent with the 90 min etching time from observation of Ru to Ti peaks in the XPS measurement. According to the previous studies, a rutile structure will be sustained when $0.025 < x < 0.75$ [2,16]. The formation of a solid solution of $V_{1-x}Ru_xO_2$ could cause the shift of RuO_2 (101) diffraction towards the higher angle as we observed [17]. It is known that transition temperature of VO_2 can be reduced by Ru doping [2,16], so the $V_{1-x}Ru_xO_2$ is expected to show a different transition temperature to the VO_2 film on top layer. Therefore we speculate that the overlap of these two transitions resulting in the two step transition in $R_n \sim T$ curves of the VO_2 film grown on RuO_2 buffered TiO_2.

Next, we consider the relative fraction of the vanadium dioxide (V^{4+}) phase. In the high resolution XPS spectra, we focused on the V $2p_{3/2}$ peaks to compare the compositional difference between various films. After the Shirley background subtraction, the V $2p_{3/2}$ peaks were de-convoluted into two peaks. At the surface, the peaks at 516.9(2) and 515.8(2) eV are assigned to V^{5+} and V^{4+}, respectively, as shown in Fig. 5a [18]. In the interior region of the film, the

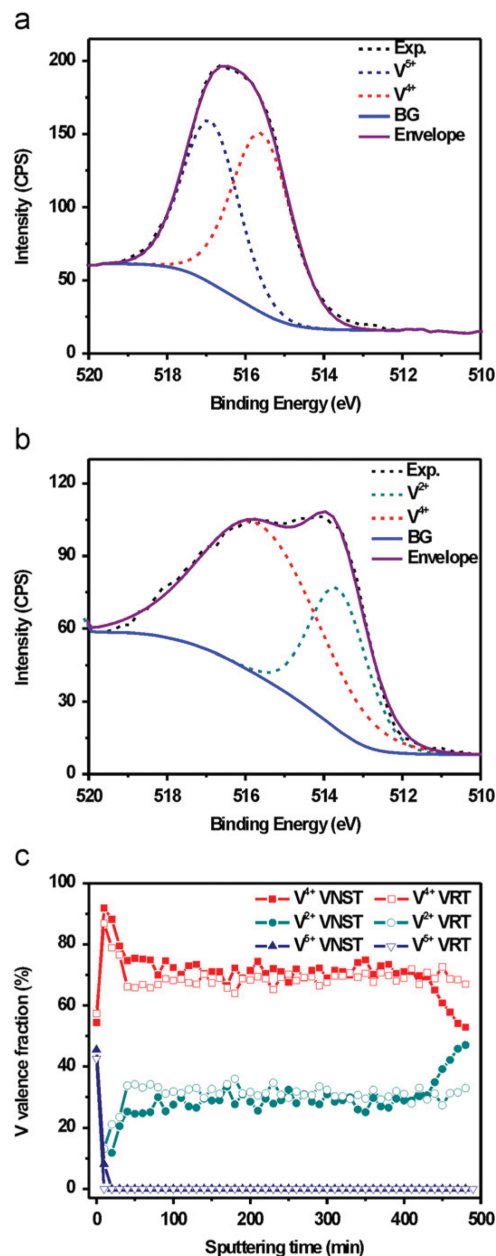

Fig. 5. De-convolution of high resolution XPS V$2p_{3/2}$ peak (a) on surface and (b) in bulk region in VO_2 film, (c) V$2p_{3/2}$ relative fraction. VNST: VO_2 on Nb doped $SrTiO_3$ and VRT: VO_2 on RuO_2 buffered TiO_2.

Author's personal copy

peaks are located at 515.8(2) eV and 513.7(2) eV and attributed to V^{4+} and V^{2+}, respectively, as shown in Fig. 5b [4,19]. The average fractions of V^{4+} for the interior region of VO_2 films are ~71% on Nb:STO and ~68% on RuO_2 buffered TiO_2, while the surface of the films are composed of about 55% of V^{4+} on both films, as shown in Fig. 5c. It also shows that the V^{4+} fraction decreased with decreasing vanadium content at the interface of VO_2 film on Nb:STO, while the V(IV) concentration was relatively unchanged for VO_2 film on RuO_2 buffered TiO_2 indicating that the V(IV) state is stabilized in the solid solution.

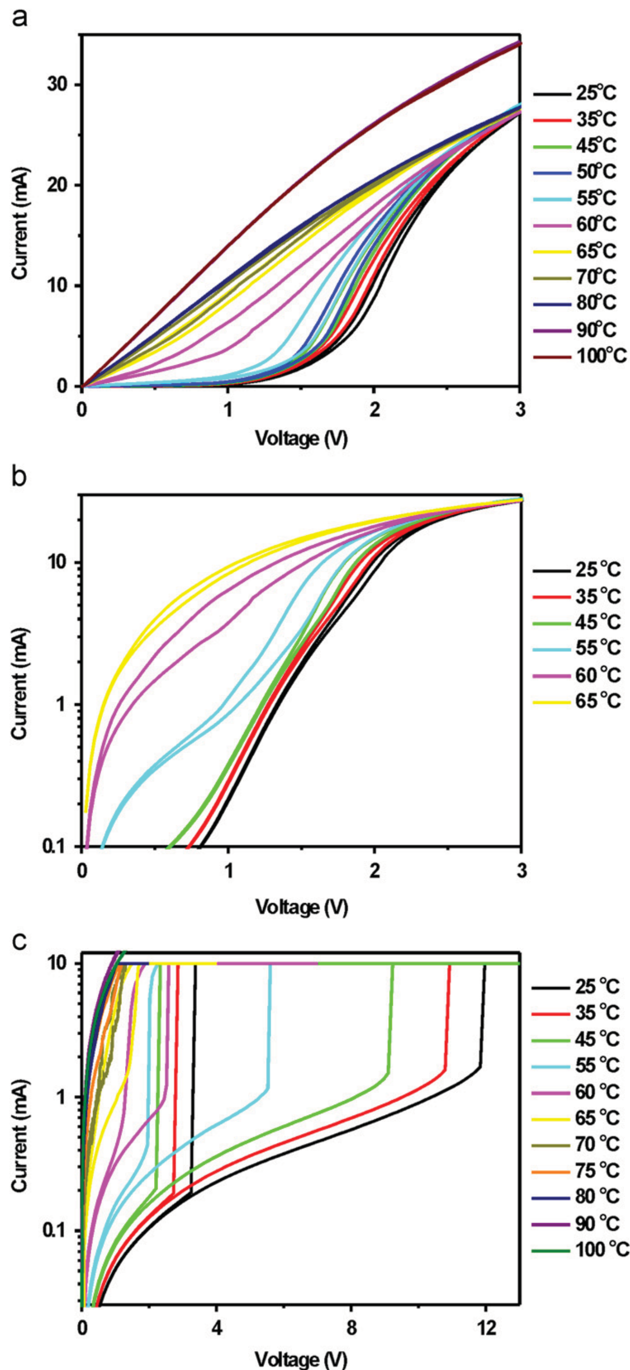

Fig. 6. Voltage-driven metal–insulator transition: (a) out-of-plane current–voltage measurement on VO2 film grown on Nb-doped $SrTiO_3$ and (b) close-up view of representative *I–V* curves at various temperatures, (c) in-plane measurement of the current–voltage curves at various temperatures.

Next, we have investigated the electrically-driven metal–insulator transition (referred to as E-MIT) with a VO_2 film grown on Nb-doped $SrTiO_3$ substrate. Experiments were carried out in both in-plane and out-of-plane geometry to understand the role of the substrate in influencing the overall current–voltage characteristics. Fig. 6(a) and (b) shows *I–V* plots measured in the out-of-plane mode (Fig. 6(b) shows the zoom-in view of fewer *I–V* curves in log scale for clarity) at different temperatures. The out-of-plane curves show a small hysteresis loop when sweeping current up and down that on its own is not clear if we can ascribe it to the phase transition. However one can get additional insights from the in-plane measurements on the same sample. In-plane results (Fig. 6(c)) show large current jumps and the threshold voltage dependence on temperature in agreement with previous studies on VO_2 [20,21]. This demonstrates that VO_2 film on Nb:STO does show the electrically-driven transition. The in-plane E-MIT happens at ~12 V, which is larger than the out-of-plane value because the spacing of electrodes in this geometry is a few tens of micrometers that is larger than the ~200 nm separation for the out-of-plane measurement. In the out-of-plane geometry, the Nb:STO substrate acts as a resistor in series with VO_2. The resistance of Nb:$SrTiO_3$ becomes larger as the voltage increases (which can be seen for example from *I–V* data at 100 °C where the resistance mainly comes from Nb:STO). When VO_2 reaches the threshold voltage for switching, there would have been a sharp current jump. However, since the *I–V* curve of Nb:STO is not linear, such a large current will need a much larger external voltage than the applied bias. As a consequence, the current only changes gradually. The larger the resistance of Nb:STO, the smaller the hysteresis loop. This is likely why the out-plane *I–V* at 55 °C has a larger hysteresis than that at 25 °C (due to decrease in resistance of Nb:STO). Although the resistance of Nb:STO continues to decrease above 60 °C, the *I–V* hysteresis becomes smaller because the E-MIT magnitude decreases as temperature increases. Similarly, the out-of-plane measurement shows a smaller metal–insulator transition magnitude than in-plane due to additional series resistance from Nb:STO substrate. The shape of the out-of-plane *I–V* curve may be explained as the following: at small voltages (~0–1.5 V) the shape is primarily determined due to the VO_2 layer contribution, which looks similar to the in-plane *I–V* curve below threshold voltage. At intermediate voltages (~1.5–2 V), the current increases gradually because of the series resistance of Nb:STO. At larger voltages (~2–3 V), the *I–V* curve corresponds to Nb:STO, and resembles *I–V* measurements at ~100 °C when the VO_2 layer is in the conducting state.

4. Summary

Textured vanadium oxide films have been grown on conducting oxide substrates by rf sputtering, and their physical properties have been studied. The VO_2 film on Nb-doped $SrTiO_3$ shows over two orders of magnitude resistance change across the transition. The VO_2 film on RuO_2 buffered TiO_2 shows a two step transition. From photoelectron spectroscopy, it is likely an interfacial $V_{1-x}Ru_xO_2$ layer is formed with a lower transition temperature resulting in the two step transition.

Acknowledgment

We are grateful to National Science Foundation Grant DMR-0952794 and Office of Naval Research Grant N00014-10-1-0131 for financial support. This work was performed in part at

Author's personal copy

the Center for Nanoscale Systems (CNS), a member of the National Nanotechnology Infrastructure Network (NNIN), which is supported by the National Science Foundation under NSF Award no. ECS-0335765.

References

[1] L.A. Ladd, W. Paul, Solid State Communications 7 (1969) 425.
[2] J.B. Goodenough, Journal of Solid State Chemistry 3 (1971) 490.
[3] D. Ruzmetov, G. Gopalakrishnan, J.D. Deng, V. Narayanamurti, S. Ramanathan, Journal of Applied Physics 106 (2009) 083702.
[4] Z. Yang, C. Ko, S. Ramanathan, Journal of Applied Physics 108 (2010).
[5] M.J. Lee, Y. Park, D.S. Suh, E.H. Lee, S. Seo, D.C. Kim, R. Jung, B.S. Kang, S.E. Ahn, C.B. Lee, D.H. Seo, Y.K. Cha, I.K. Yoo, J.S. Kim, B.H. Park, Advanced Materials 19 (2007) 3919.
[6] T.H. Yang, C.M. Jin, H.H. Zhou, R.J. Narayan, J. Narayan, Applied Physics Letters 97 (2010) 702101.
[7] J.S. Becker, E. Kim, R.G. Gordon, Chemistry of Materials 16 (2004) 3497.
[8] D. Ruzmetov, K.T. Zawilski, V. Narayanamurti, S. Ramanathana, Journal of Applied Physics 102 (2007) 113715.
[9] F. Swanson, National Bureau of Standards (U.S.) Circular 3 (1953) 539.
[10] I.E. Grey, C. Li, C.M. MacRae, L.A. Bursill, Journal of Solid State Chemistry 127 (1996) 240.
[11] C.E. Boman, Acta Chemica Scandinavica 24 (1970) 116.
[12] K.D. Rogers, Powder Diffraction 8 (1993) 240.
[13] G. Schön, Journal of Electron Spectroscopy 1 (1972) 377.
[14] S. Oswald, W. Brückner, Surface and Interface Analysis 36 (2004) 17.
[15] P.C. Liao, S.Y. Mar, W.S. Ho, Y.S. Huang, K.K. Tiong, Thin Solid Films 287 (1996) 74.
[16] B.L. Chamberland, D.B. Rogers, Patent in U.S., 1970, Patent No. 3,542,697.
[17] K. Yokoshima, T. Shibutani, M. Hirota, W. Sugimoto, Y. Murakami, Y. Takasu, Journal of Power Sources 160 (2006) 1480.
[18] G.A. Sawatzky, D. Post, Physical Review B 20 (1979) 1546.
[19] D.H. Youn, H.T. Kim, B.G. Chae, Y.J. Hwang, J.W. Lee, S.L. Maeng, K.Y. Kang, Journal of Vacuum Science & Technology A 22 (2004) 719.
[20] H.T. Kim, B.G. Chae, D.H. Youn, G. Kim, K.Y. Kang, S.J. Lee, K. Kim, Y.S. Lim, Applied Physics Letters 86 (2005) 242101.
[21] C. Ko, S. Ramanathan, Applied Physics Letters 93 (2008) 252101.